Research Square

Preprints are preliminary reports that have not undergone peer review.
They should not be considered conclusive, used to inform clinical practice,
or referenced by the media as validated information.

Synergistic Study of Electrocatalytic activity and Corrosion Stability of Ni-W Alloy Coatings on Copper Substrates for Alkaline Water Splitting

Samir Safarov

samirsfrovchemistry19@gmail.com

Institute of Chemistry PLE, Ministry of Science and Education of the Republic of Azerbaijan, AZ 1143, Baku, H. Javid 113, Baku, Azerbaijan

Ruhangiz Guseinova

Institute of Chemistry PLE, Ministry of Science and Education of the Republic of Azerbaijan, AZ 1143, Baku, H. Javid 113, Baku, Azerbaijan

Akif Aliyev

Institute of Chemistry PLE, Ministry of Science and Education of the Republic of Azerbaijan, AZ 1143, Baku, H. Javid 113, Baku, Azerbaijan

Natavan Soltanova

Institute of Chemistry PLE, Ministry of Science and Education of the Republic of Azerbaijan, AZ 1143, Baku, H. Javid 113, Baku, Azerbaijan

Dunya Babanly

French-Azerbaijani University, Azerbaijan State Oil and Industry University, AZ1000, Baku, Azerbaijan, Nizami str. 183, Baku, Azerbaijan

Aygun Zeynalova

Institute of Chemistry PLE, Ministry of Science and Education of the Republic of Azerbaijan, AZ 1143, Baku, H. Javid 113, Baku, Azerbaijan

Telli Hamzayeva

Institute of Geology and Geopolitics, Ministry of Science and Education of the Republic of Azerbaijan, AZ 1073, Baku, H. Javid 119 , Baku, Azerbaijan

Shafag Bayramova

Institute of Geology and Geopolitics, Ministry of Science and Education of the Republic of Azerbaijan, AZ 1073, Baku, H. Javid 119 , Baku, Azerbaijan

Dilgam Tagiyev

Institute of Chemistry PLE, Ministry of Science and Education of the Republic of Azerbaijan, AZ 1143, Baku, H. Javid 113, Baku, Azerbaijan

---

Research Article

Keywords: electrocatalyst, nickel, tungsten, HER, corrosion

Posted Date: June 15th, 2026

DOI: https://doi.org/10.21203/rs.3.rs-9812047/v1

License: This work is licensed under a Creative Commons Attribution 4.0 International License.
Read Full License

Additional Declarations: No competing interests reported.

Synergistic Study of Electrocatalytic activity and Corrosion Stability of Ni-W Alloy Coatings on Copper Substrates for Alkaline Water Splitting

Samir Safarov[1*], Ruhangiz Guseinova[1], Akif Aliyev[1], Natavan Soltanova[1], Dunya Babanly[3], Aygun Zeynalova[1], Telli Hamzayeva[2], Shafag Bayramova[2], Dilgam Tagiyev [1]

[1]Institute of Chemistry PLE, Ministry of Science and Education of the Republic of Azerbaijan, AZ 1143, Baku, H. Javid 113, Baku, Azerbaijan

[2]Institute of Geology and Geopolitics, Ministry of Science and Education of the Republic of Azerbaijan, AZ 1073, Baku, H. Javid 119 **,** Baku, Azerbaijan

[3]French-Azerbaijani University, Azerbaijan State Oil and Industry University, AZ1000, Baku, Azerbaijan, Nizami str. 183, Baku, Azerbaijan

Email: Samir Safarov[*]**-samirsfrovchemistry19@gmail.com**

* Corresponding author

Abstract: Due to the increasing use of fossil fuels and their harmful impact on the environment, researchers are developing methods for producing environmentally friendly hydrogen that can effectively replace them. There are many methods for producing clean hydrogen, one of which is water electrolysis. Transition metal-based electrocatalysts play an important role in water electrolysis, serving as an alternative to expensive noble metals.In this work, the electrocatalytic and corrosion properties of Ni–W alloy coatings obtained by electrodeposition from a citrate electrolyte for the hydrogen evolution reaction are presented. X-ray diffraction analysis showed that the co-deposition of Ni with W leads to the formation of the chemical compound Ni_4W on the cathode surface. By recording linear polarization curves and subsequently constructing Tafel plots, the effect of tungsten content in the thin film on its electrocatalytic and corrosion properties was investigated. It was found that the films denoted in the article as Ni–$W_{0.04}$, with a tungsten content of 23.24 wt% and a geometric surface area of 2 cm^2, exhibited a Tafel slope of 93 mV dec^{-1} and a corrosion rate of 0.528 mm/year, demonstrating the best electrocatalytic and corrosion properties in an alkaline medium.

Key words: electrocatalyst, nickel, tungsten, HER, corrosion

1 Introduction

As fossil fuel reserves are depleted and the demand for renewable energy increases, research into sustainable energy sources is becoming increasingly important. Green hydrogen is a clean energy source and a promising alternative to fossil fuels, whose use leads to greenhouse gas emissions into the atmosphere [1,2]. In addition to its use as a fuel, hydrogen is also important in industries such as oil refining and ammonia production [3–6]. This represents a global challenge that requires efficient large-scale hydrogen production methods. Although various hydrogen production methods are available, including steam reforming, coal gasification, and photoelectrochemical water splitting, steam reforming remains the dominant approach. However, due to high temperatures and significant CO_2 emissions, this process is neither economically nor environmentally viable [7]. Due to its high energy efficiency, environmental friendliness, and ability to produce pure hydrogen, water electrolysis has recently attracted significant attention from researchers as one of the most affordable, safe, and accessible methods of hydrogen production. This process involves two reactions: hydrogen evolution at the cathode (HER) and oxygen evolution at the anode (OER). The main challenge is the high energy consumption caused by slow reaction kinetics and the required potential (1.8–2.4 V), which significantly exceeds the theoretical value (1.23 V).Although noble metals and their oxides are currently the best electrocatalysts, their scarcity and high cost limit widespread industrial application. As a result, only about 4% of global hydrogen production is currently obtained via water electrolysis [8]. Considering that hydrogen is most commonly produced industrially from alkaline electrolytes, most studies focus on water electrolysis in alkaline solutions. Due to the stability of transition metals and their alloys in alkaline electrolytes, they are preferred for industrial hydrogen production, replacing platinum and other noble metals as electrodes for the hydrogen evolution reaction [9–12]. Recently, research has increasingly focused on the development of transition metal-based electrocatalysts for water electrolysis due to their improved catalytic properties, activity, enhanced stability, excellent corrosion resistance, and low production cost [13,14]. Among these, nickel-based catalysts used in various forms (mesh, felt, and foam) demonstrate the best performance and are widely employed in large-scale applications. It is known that tungsten and molybdenum are two metals that cannot be electrodeposited from aqueous electrolytes. The deposition of these metals is only possible through induced co-deposition [15]. In studies [16,17], the authors suggest that the co-deposition of Ni with W in a citrate electrolyte occurs via their complex compound $[NiCitWO_2]^-_ad_s$. Citrate

electrolytes are used for the deposition of tungsten with other elements, as they promote an increased tungsten content in the deposit [18,19].In this work, the electrocatalytic and corrosion properties of a Ni–W alloy coatings obtained by electrochemical deposition on a copper substrate from an acidic citrate electrolyte are investigated.In this paper, the influence of tungsten content on such important properties of electrocatalysts as morphology, structure, crystallite size, electrocatalytic activity, corrosion resistance and stability of Ni-W alloys obtained by electrolysis was investigated.

2 Experimental

The samples were synthesized on a copper plate substrate with a geometric surface area of 2 cm^2 for three samples and 0.5 cm^2 for one sample. The reagents used for the **synthesis of the thin films were $NiSO_4$, $(NH_4)_4W_5O_7$, $Na_3C_6H_5O_7$, and H_3BO_3, all obtained** from Sigma-Aldrich (Germany). Before deposition, the copper substrate was etched in an HNO_3:H_2O (1:1) solution, then rinsed with distilled water, ethanol, and acetone.

2.1 Electrolyte preparation

The electrolyte for the co-deposition of nickel and tungsten consisted of 0.08 M $NiSO_4$, 0.2 M $Na_3C_6H_5O_7$, 0.1 M H_3BO_3, and $(NH_4)_4W_5O_7$ at three different concentrations: 0.01 M, 0.03 M, and 0.04 M. The resulting thin films are hereafter referred to as Ni–$W_{0.01}$ (a), Ni–$W_{0.03}$ (b), and Ni–$W_{0.04}$ (c). Sodium citrate was used as a complexing agent, and H_3BO_3 as a buffering component. To prepare the electrolytes, the weighed amounts of the initial reagents were sequentially dissolvd in 50 mL of distilled water at 333 K under stirring with a magnetic stirrer for 10–20 minutes until a clear solution was obtained. After preparation, the pH of the electrolyte was measured and found to be 4.2 for each solution.

2.2 Electrodeposition of Ni–W alloys

The samples for investigation were obtained by electrochemical deposition in galvanostatic mode. The electrodeposition process was carried out on a copper plate at a current density of 20 mA cm^{-2} for 30 minutes at a temperature of 323 K. Platinum (Pt) with a surface area of 4 cm^2 was used as the anode. After electrodeposition, the samples were rinsed with distilled water and dried at room temperature. Since nickel is

a component of the deposited film, copper was chosen as the substrate. Furthermore, copper has high electrical conductivity, is easy to surface treat before deposition, and is low cost, which is important for electrocatalysts in water electrolysis. The electrodeposition conditions were selected based on preliminary studies. Increasing the current density above 20 mA/cm^2 resulted in the deposition of loose deposits that were poorly adhered to the substrate surface. The optimal current density for deposition was 15–20 mA/cm^2.

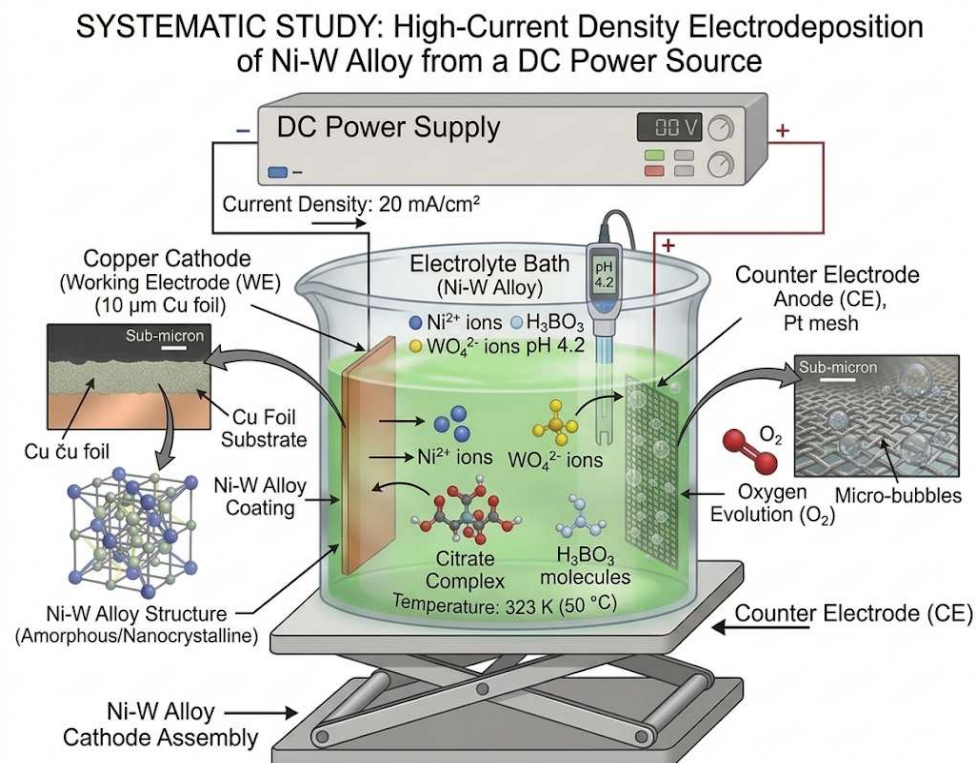


Fig.1 Schematic representation of the two-electrode electrochemical cell. Schematic diagram of the electrochemical setup used for galvanostatic electrodeposition of a Ni–W alloy coating on a copper substrate. The deposition was carried out at a current density of 20 mA cm^{-2} and a temperature of 323 K. The figure also illustrates the electrolyte composition and configuration of the working and counter electrodes.

The thickness of the electrodeposited Ni–$W_{0.04}$ specimen was measured as 9.29 µm, playing a pivotal role in governing the long-term corrosion resistance of the alloy coating.

2.3 Electrochemical studies

The electrocatalytic properties of the synthesized samples were investigated in a three-electrode electrochemical cell. A platinum electrode was used as the counter electrode,

and an Ag/AgCl electrode in saturated KCl solution was used as the reference electrode. The electrocatalytic properties of the obtained samples were studied in a 1 M KOH solution. Linear sweep voltammetry (LSV) measurements and chronopotentiometric studies were carried out using an IVIUMSTAT Electrochemical Interface potentiostat at a temperature of 298 K and a scan rate of 5 mV/s. Stability tests of the electrocatalysts and corrosion properties were evaluated by the chronopotentiometric method at a current density of 10 mA/cm² for 24 hours. Corrosion values were obtained by constructing Tafel plots. The surface morphology and elemental composition of the synthesized samples were determined using a scanning electron microscope (SEM) from JEOL (Japan), equipped with an energy-dispersive X-ray spectrometer (EDX) from Oxford Instruments. The phase composition of Ni–$W_{0.04}$ after annealing at 773 K for 1.5 hours was determined by X-ray diffraction (XRD) analysis.

3 Results and discussion

3.1 X-ray diffraction analysis of Ni–W alloys

The activity of an electrocatalyst is directly related to its electronic structure, the number of active sites, and surface morphology. The complexation of metal ions with ligands during synthesis has a decisive influence on these parameters. Nickel and tungsten complexes formed during deposition in the presence of sodium citrate slow down the reduction kinetics of nickel ions.

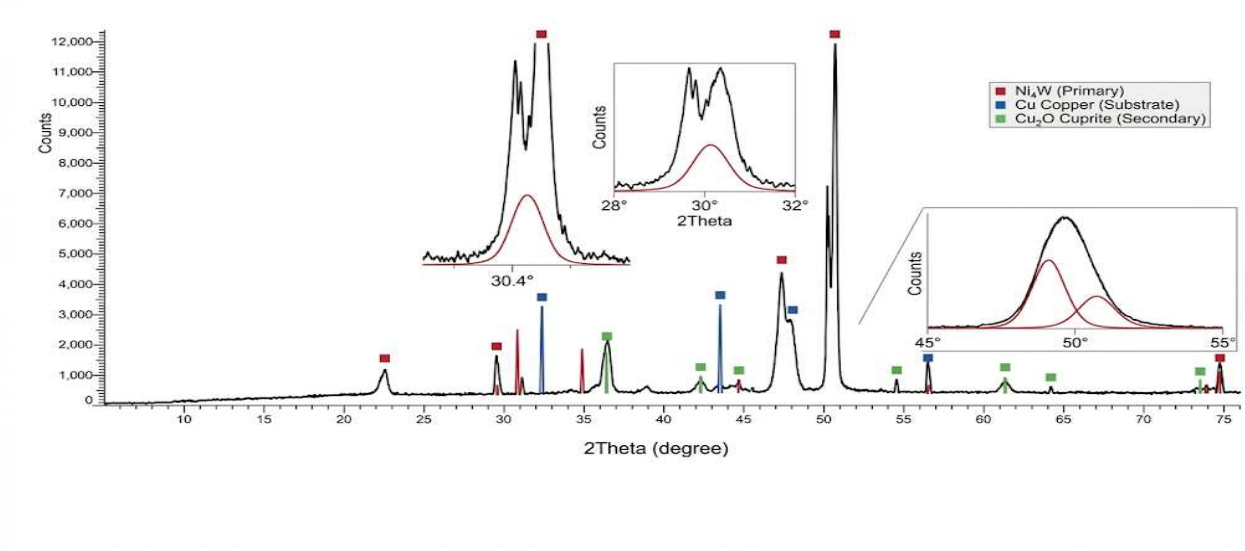


Fig.2 X-ray diffraction pattern of the Ni–$W_{0.04}$ alloy coating on a copper substrate. The XRD pattern illustrates the crystalline phases present in the deposited Ni–$W_{0.04}$ alloy

coating. The red, blue, and green squares indicate the diffraction peaks corresponding to the Ni_4W phase, the Cu substrate, and the Cu_2O phase, respectively.

The incorporation of tungsten into the film changes the d-electron density of nickel, leading to the formation of intermediate hydrogen species. This effect increases the rate of the Volmer–Heyrovsky step in the hydrogen evolution reaction (HER) and reduces the overpotential. To determine the phase composition of the sample, X-ray diffraction analysis was performed (Fig. 2). The diffraction pattern shows two copper phases, Cu_2O and Cu, which are associated with the substrate material. It can be seen that co-deposition leads to the formation of the chemical compound Ni_4W, whose peaks are relatively weak even when compared with reference peaks and correspond to its intermetallic phase. In some cases, the Ni_4W peaks overlap with those of Cu_2O, indicating that after annealing, the Ni_4W phase has not yet fully crystallized and represents a partially formed intermetallic phase close to the fully developed one [20] X-ray diffraction analysis shows that Ni_4W peaks (red lines) are observed in the regions of 30°, 50°, and 75°, confirming that the sample mainly consists of Ni_4W. Cu peaks (blue lines) are observed at 43° and 50°, which is explained by the substrate material. Cu_2O peaks (green lines), observed at 35° and 60–65°, indicate the oxidation of part of the copper substrate. The formation of copper(I) oxide occurs due to the contact of the sample with air during heat treatment, as well as the tendency of copper to oxidize easily. To obtain a fully ideal intermetallic Ni_4W phase, the elemental ratio should be 4:1. However, the fact that the film is deposited on copper, which tends to oxidize rapidly, hinders the formation of a fully intermetallic phase. The structural characteristics of the synthesized Ni–$W_{0.04}$ alloy coating were comprehensively evaluated via X-ray diffraction (XRD) analysis, with the calculated parameters summarized in Table 1. The diffraction patterns confirm that Ni_4W serves as the primary catalytic phase, exhibiting a tetragonal crystal structure with lattice constants of a = 5.732 Å and c = 3.554 Å. Additionally, a secondary Cu_2O phase (cuprite) was identified, which is attributed to the interfacial oxidation of the copper substrate during thermal treatment. The calculated crystallite size for the Ni_4W phase ranges between 10 and 15 nm, indicating a nanostructured morphology that is conducive to enhanced electrocatalytic activity.

Table. 1 Calculated lattice parameters, crystallite sizes, and Miller indices of the Ni–$W_{0.04}$ alloy coating derived from XRD analysis

Phase	Crystal system	Miller index(hkl)	Lattice parameter (Å)	Scherrer crystallite size / nm	Notice
Ni_4W	Tetragonal	(111),(020),(211)	a=5.732 **Å,**c=3.554 **Å**	10-15 nm	Main phase
Cu	Cubic	(111), (200)	a=3.612 **Å**	>50 nm	Substrate
Cu_2O	Cubic	(111),(200),(220)	a=4.268 **Å**	15-25 nm	Oxidized transition layer

The volume of the tetragonal lattice for the Ni_4W phase is determined using the following relation:

$$V = a^2 c = 5.732 \cdot 3.554 = 116.77 \text{ Å}^3$$

116.77 $Å^3$ value slightly exceeds that of the standard Ni_4W phase, indicating a higher density of active sites on the catalyst surface. Furthermore, the calculated lattice parameters exhibit notable deviations from the standard values, which is primarily attributed to internal stress within the crystal structure.

3.2 SEM and EDX analysis of alloys

SEM analysis was used to study the surface morphology of the synthesized samples, providing extensive information about the surface structure of the electrocatalysts. Figure 3 shows SEM results for three Ni–W thin film samples with different tungsten contents. As seen from the figure, a high tungsten content on the electrode surface increases its roughness and heterogeneity, which affects the electrocatalytic efficiency of water splitting [21,22]. The surface of the Ni–$W_{0.01}$ sample appears more granular and uniform. As the concentration of tungsten ions increases in Ni–$W_{0.03}$, specific clusters and protrusions begin to form on the surface. The analysis shows that the surface of the Ni–$W_{0.04}$ sample is rougher and more pronounced compared to the other two samples. It can be concluded that increasing the concentration of tungsten ions leads to higher roughness, heterogeneity, and porosity of Ni–W thin films, which contributes to an increase in the electrochemically active surface area (ECSA). This significantly affects the electrocatalytic properties and stability of the electrocatalyst. SEM analysis showed a gradual increase in crystallite size from sample a) to sample c). The average size of structural elements with increasing W content in the alloys increases from approximately 0.5–1.5 μm to 3–6 μm and is accompanied by a transition from a fine-grained dense structure to a coarser-grained and heterogeneous surface morphology.

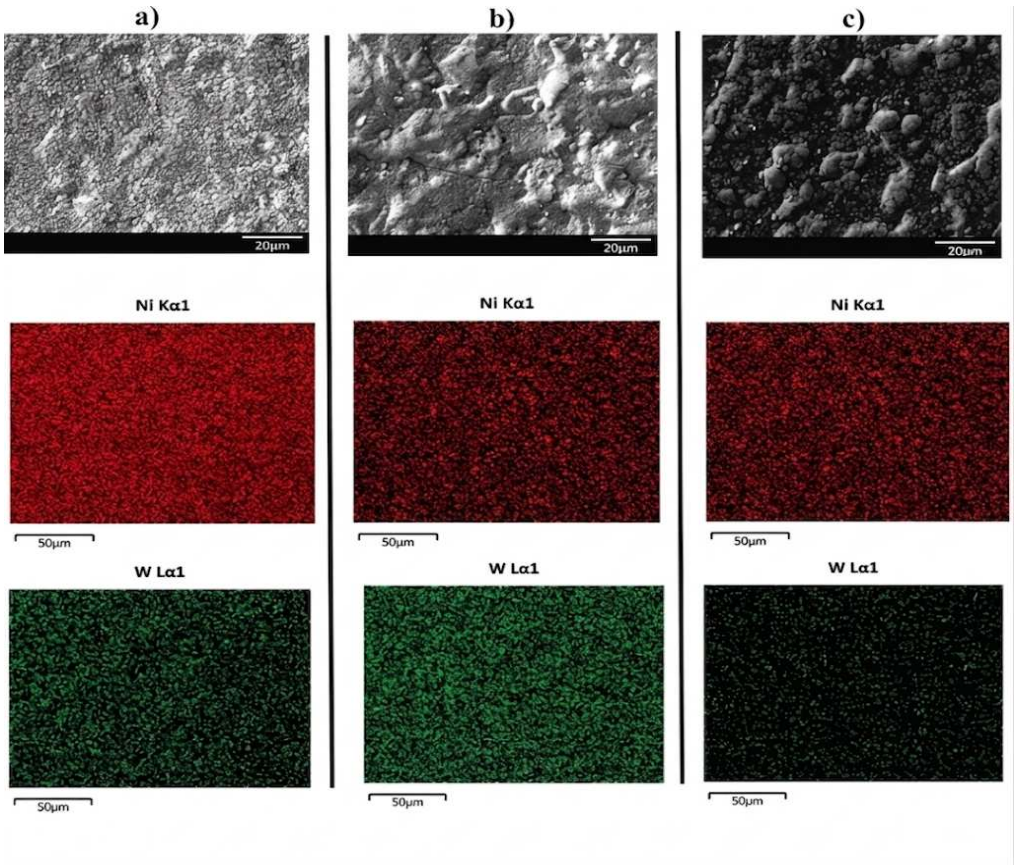


Fig.3 SEM images of Ni–W alloy coatings.(a–c) SEM micrographs of Ni–$W_{0.01}$, Ni–$W_{0.03}$, and Ni–$W_{0.04}$ coatings, respectively. In panels (d–f), the EDS maps for Ni ($K\alpha_1$) show a uniform distribution (red color). In panels (g–i), the EDS maps for W ($L\alpha_1$) demonstrate an increasing tungsten concentration and homogeneous dispersion (green color) with increasing tungsten content. The scale bars in (a–c) correspond to 20 µm. All EDS analyses were performed on cross-sections to evaluate elemental distribution and uniformity.

Ni-$W_{0.01}$ (a), Ni-$W_{0.03}$ (b) and Ni-$W_{0.04}$ (c).

As seen in Figure 4, nickel ($K\alpha_1$) and tungsten ($L\alpha_1$) are uniformly distributed over the substrate surface in all three samples, with an increasing tungsten content in the deposits from left to right (green color). Figure 4 presents the EDX analysis results for all three Ni–W thin film samples with different tungsten contents. In all three spectra, the peaks of Ni and W are clearly visible. The small amount of carbon (C) and oxygen (O) peaks is attributed to their adsorption from the atmosphere and surface oxidation of the films.

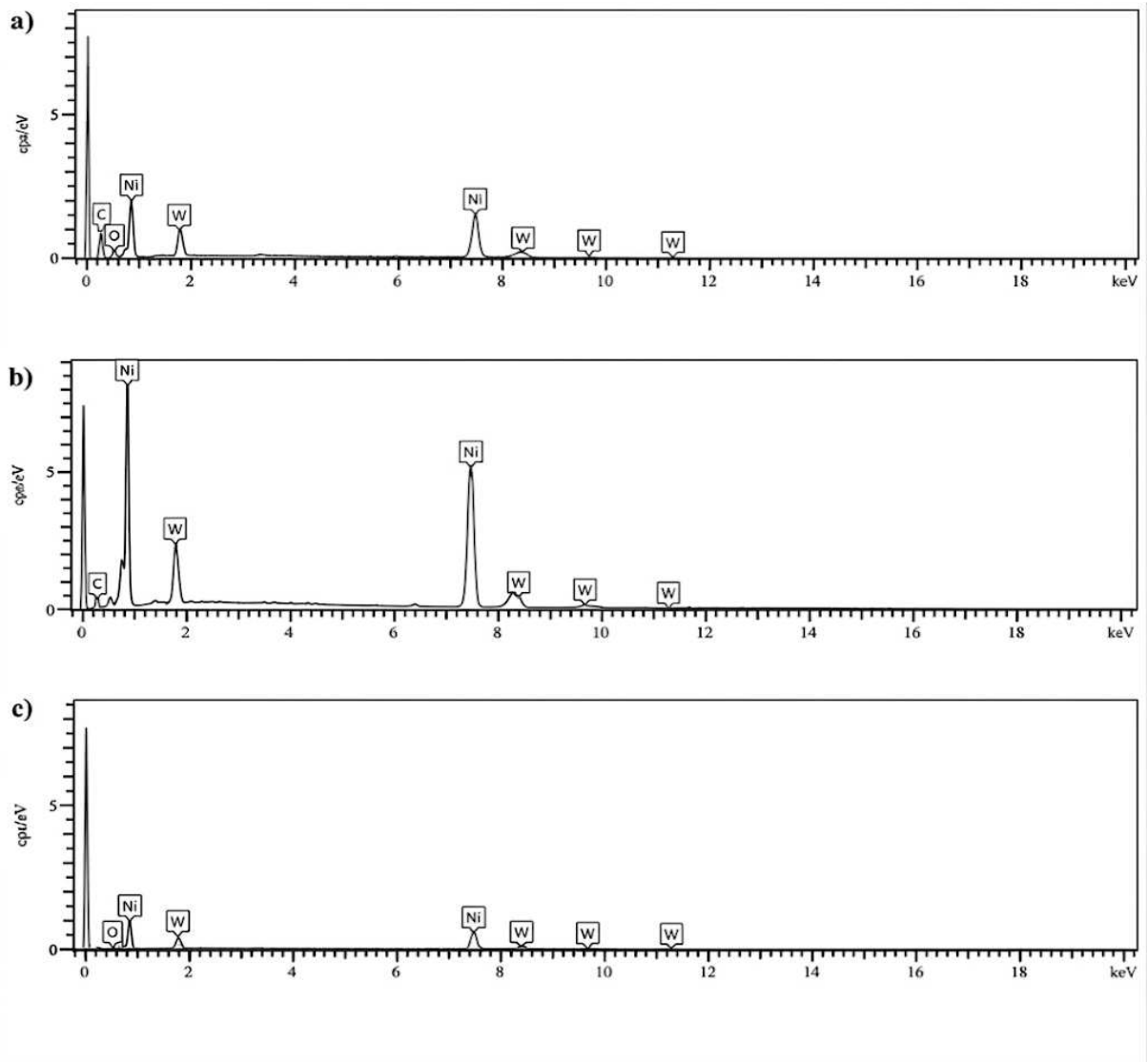


Fig.4 EDX spectra of Ni–W alloy coatings with different tungsten contents. EDX spectra of Ni–W coatings with different compositions: Ni–$W_{0.01}$ (a), Ni–$W_{0.03}$ (b), and Ni–$W_{0.04}$ (c). The spectra confirm the presence of nickel and tungsten and show variation in tungsten content among the samples.

Table 2 presents the quantitative composition of all three Ni–W alloy samples with different tungsten contents.

Table. 2 EDX quantitative analysis of Ni-W alloys

Element	Ni-$W_{0.01}$	Ni-$W_{0.03}$	Nickel-$W_{0.04}$
Nickel	31.80 %	52.77 %	55.65 %
Wolfram	9.40 %	12.28 %	23.24 %
Oxygen	45.74 %	30.21 %	21.21 %
Carbon	12.99 %	4.74 %	-

As can be seen from Table 2, all samples contain oxygen, which is produced by annealing in air. According to current literature, oxide electrocatalysts based on Co, Ni, Fe, and mixed oxides exhibit high activity in water electrolysis. A significant increase in catalytic

activity is achieved through the creation of oxygen vacancies, doping with transition metals, and the formation of heterostructured surfaces. EDX analysis shows that with increasing tungsten content in the sample, the intensity of the nickel peak decreases, which is related to the atomic weight of tungsten. Being a heavy element, tungsten strongly scatters the incident electron beam and absorbs nickel signals. Another issue is associated with electrochemical deposition, in which a very high amount of energy is transferred to the system, leading to the formation of a metastable phase. In a metastable phase, the system has high energy and remains in a non-equilibrium state. During electrodeposition, atoms are arranged so closely that they do not have sufficient time to form an ordered structure, remaining in a strained state and creating microdeformations known as internal stress. This results in the formation of a large number of defects, which enhance the electrocatalytic activity of the electrocatalyst. It is known that water electrolysis consists of three stages: Volmer, Heyrovsky, and Tafel. All three equations describing the hydrogen evolution reaction steps are given below [23,24].

$$H_2O + e^- + M \rightarrow M\text{-}H_{ads} + OH^- \quad \text{Volmer step (b=-120 mV dec}^{-1}\text{)} \quad (1)$$

$$M\text{-}H_{ads} + H_2O + e^- \rightarrow M + H_2 + OH^- \quad \text{Heyrovsky step (b=-40mV dec}^{-1}\text{)} \quad (2)$$

$$2\ M\text{-}H_{ads} \rightarrow 2M + H_2 \quad \text{Tafel step (b=-30 mV dec}^{-1}\text{)} \quad (3)$$

The formation of a metastable phase facilitates water electrolysis by generating a large number of active sites, which enhance the electrocatalytic activity of the catalyst and reduce the Tafel slope [25]. This leads to the predominance of the Volmer–Heyrovsky pathway and very rapid hydrogen adsorption.

3.3 Electrocatalytic activity of coatings in the hydrogen evolution reaction

The electrocatalytic activity of the Ni–W electrocatalyst was investigated by recording linear polarization curves in 1 M KOH solution at room temperature (Fig. 5). The experiment was carried out using three different samples with a constant nickel content but varying tungsten concentrations. In addition, designated as $Ni–W_{0.04}$ in the figure, was also tested and showed high catalytic activity more than other samples in 1 M KOH solution. According to the Sabatier principle, the M–H bond energy is relatively close to the peak of the Ni volcano plot. The addition of tungsten modifies the electron density, leading to a decrease in the Tafel slope [26–28].

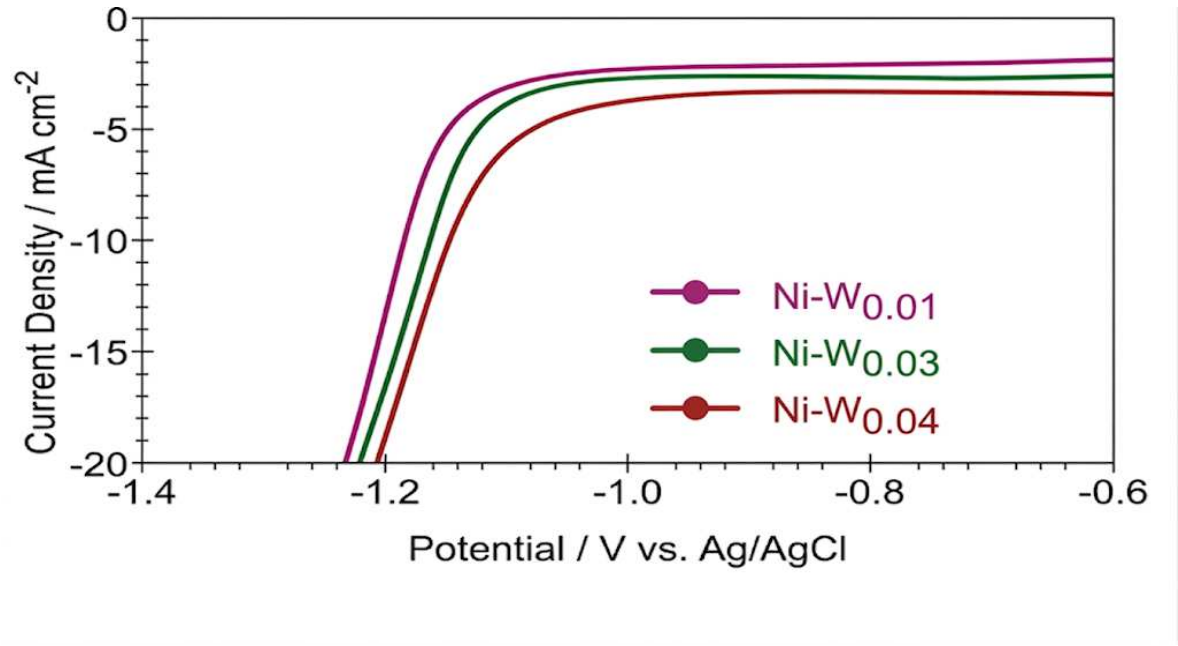


Fig.5 Linear sweep voltammetry curves of Ni–W alloy coatings. LSV curves of Ni–W alloy coatings recorded in 1 M KOH at 298 K with a scan rate of 5 mV s^{-1}, illustrating the electrocatalytic behavior of the samples.

The electrochemical parameters obtained from linear voltammetry data were fitted into the Tafel equation. The studies showed that an increase in tungstate ion concentration in the Ni–W alloy has a positive effect on the electrocatalyst properties, leading to a decrease in the Tafel slope. Such high efficiency is attributed to the large real surface area and high density of active sites in the alloy [29–31]. It was established that increasing the tungsten content in the Ni–W thin film enhances the efficiency of the electrocatalyst in the hydrogen evolution reaction (HER). Most likely, tungsten ions modify the electronic structure of the alloy, which is crucial for HER performance. In addition, increasing tungsten content significantly affects the amorphous nature of the electrocatalyst [32]. As mentioned earlier, the alloys were deposited on a pure copper electrode. According to the Sabatier principle, pure copper is poorly suited for the HER because it weakly binds H^+, which hinders proton adsorption. However, nickel and tungsten ions deposited on its surface facilitate this process, and the Volmer–Heyrovsky mechanism becomes dominant. The Ni–W alloys on the copper electrode—Ni–$W_{0.01}$ (a), Ni–$W_{0.03}$ (b) showed Tafel slope values of 118 and 109 mV dec^{-1}, respectively, while the Ni–$W_{0.04}$ sample exhibited a Tafel slope of 93 mV dec^{-1}. The good electrical conductivity of copper and the large electrochemically active surface area of the Ni–W alloy contribute to the reduced Tafel slope compared to a pure nickel electrode [33,34].

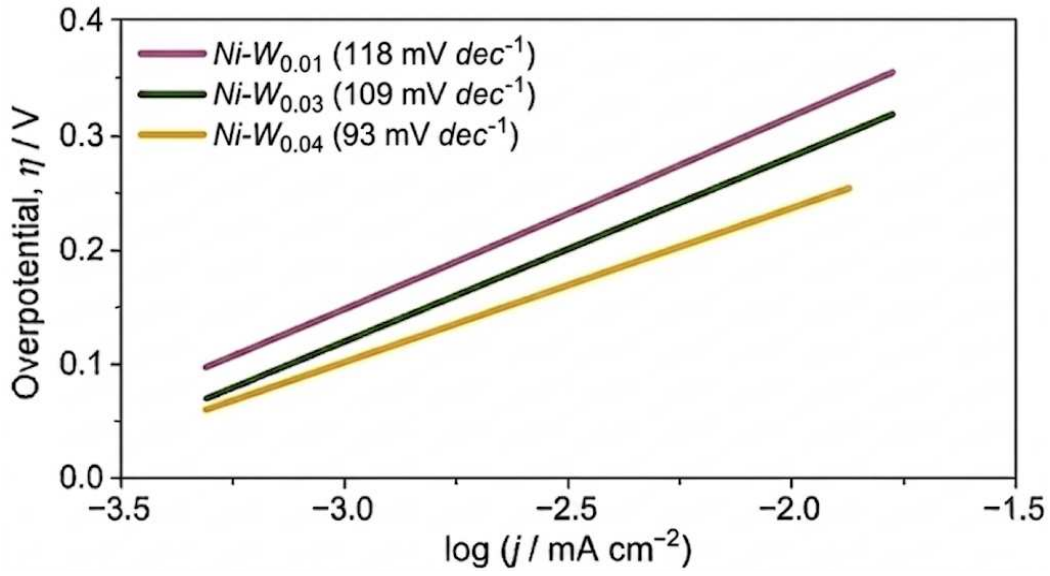


Fig.6 Tafel plots of Ni–W alloy coatings for the hydrogen evolution reaction.

Tafel plots of Ni–W coatings with different compositions obtained from polarization measurements in 1 M KOH solution, used to evaluate the kinetics of the hydrogen evolution reaction (HER).

Apparently, the real surface areas of these samples are close to each other; however, the density of active sites in the Ni–$W_{0.04}$ sample is higher, which significantly affects the Tafel slope [35,36].

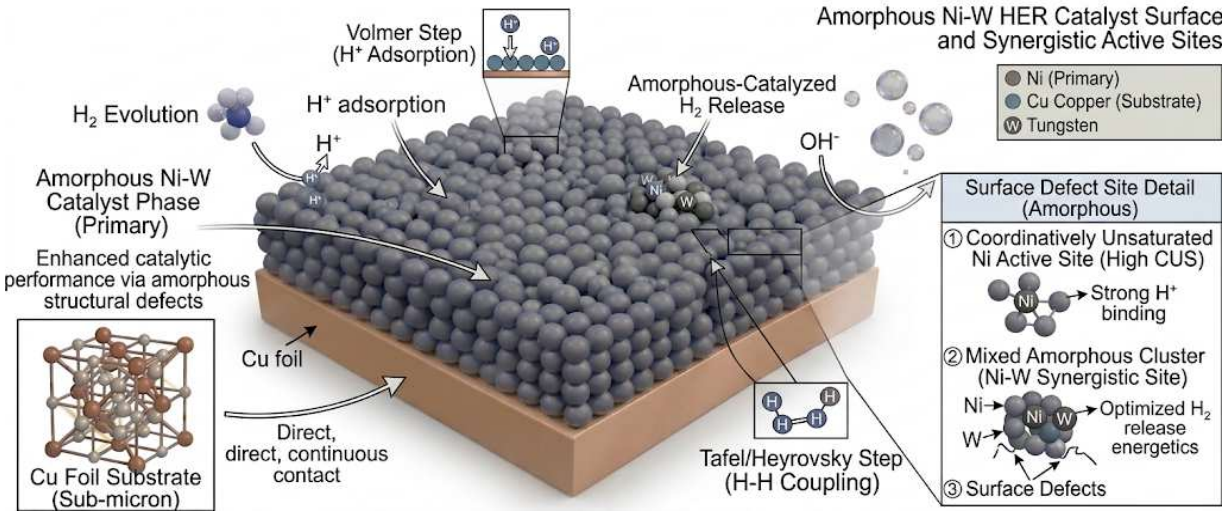


Fig 7. Schematic illustration of the hydrogen evolution reaction (HER) mechanism on the surface of the amorphous Ni–W catalyst electrodeposited on a Cu foil substrate. The diagram highlights the disordered atomic structure characterized by abundant surface defects and coordinatively unsaturated sites (CUS).

The multi-step alkaline HER pathway is depicted, showcasing the initial water dissociation and proton adsorption (Volmer step) followed by molecular hydrogen coupling and release (Tafel/Heyrovsky step) over the synergistic Ni–W active clusters. The direct, continuous contact with the underlying sub-micron Cu foil substrate ensures efficient electron transport during high-rate electrolysis.

Apparently, the real surface areas of these samples are close to each other; however, the density of active sites in the Ni–$W_{0.04}$ sample is higher, which significantly affects the Tafel slope [35,36].The electrochemical and kinetic parameters of Ni–W samples with different compositions are presented in Table 3. The table shows the values of the exchange current density (j_0), which represents the reaction rate at equilibrium, the overpotentials at 10 mA cm^{-2} and 100 mA cm^{-2}, as well as the Tafel slope values for each of the four samples.

Table.3 Electrochemical kinetic parameters obtained from Tafel plots for different Ni–W alloys in 1 M KOH.

Test sample	Tafel slope(b)	j_0(mA cm^{-2})	η_{10}(mV)	η_{100}(mV)
Ni-$W_{0.01}$	118 mV dec^{-1}	7.9 x 10^{-5}	318	436
Ni-$W_{0.03}$	109 mV dec^{-1}	1.2 x 10^{-4}	272	381
Ni-$W_{0.04}$	93 mV dec^{-1}	2 x 10^{-4}	224	317

By comparing the kinetic and electrochemical parameters of all four samples, it can be concluded that the Ni–$W_{0.04}$ sample exhibits the best electrocatalytic performance compared to the other samples in the hydrogen evolution reaction.

3.4 Cyclic voltammetry (CV)

Figure 8 shows cyclic voltammetry curves in different scan rates.

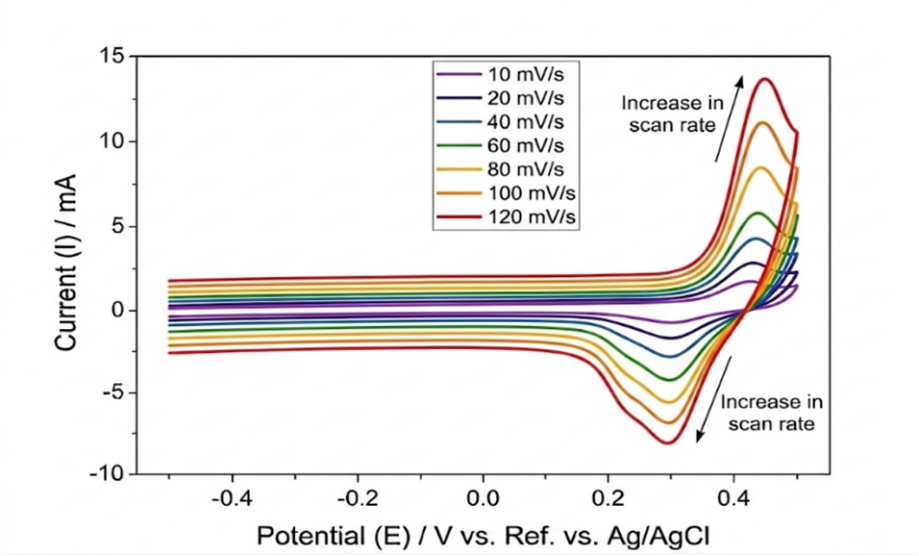


Fig. 8 CV curves Ni–$W_{0.04}$ alloy coating, 1 M KOH and 298 K

The cyclic voltammetry (CV) profiles reveal a well-defined redox couple, where the anodic peak observed at approximately 0.45 V corresponds to the oxidation of $Ni(OH)_2$ to NiOOH, while the cathodic peak at circa 0.30 V signifies the subsequent reduction of NiOOH back to $Ni(OH)_2$. As the scan rate increases from 10 mV/s to 120 mV/s, a progressive shift in the peak potentials is observed: the anodic peaks shift toward more noble (positive) potentials, and the cathodic peaks migrate toward more negative values. This phenomenon indicates the emergence of kinetic limitations at higher sweep rates, primarily attributed to ohmic polarization and mass transfer constraints within the nanostructured electrode. Furthermore, the increasing peak potential separation with the scan rate confirms the quasi-reversible nature of the electrochemical redox process on the synthesized Ni–$W_{0.04}$ surface.

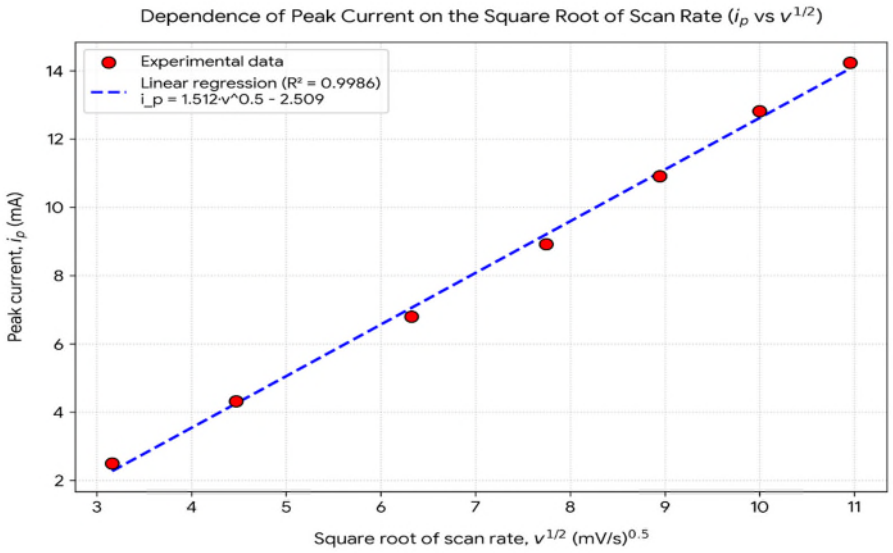


Fig.9 Dependence of Peak Current on the Square Root of Scan rate (i_p vs $v^{1/2}$)

Figure 9 illustrates the linear dependence of the peak current (i_p) on the square root of the scan rate ($v^{1/2}$) for the hydrogen evolution reaction (HER) in a 1 M KOH electrolyte. As clearly observed from the plots, the peak current scales linearly with $v^{1/2}$, which rigorously demonstrates that the electrocatalytic process is governed by a diffusion-controlled mechanism. This behavior implies that even if the electrocatalyst possesses exceptionally high intrinsic catalytic activity, the overall reaction rate is ultimately restricted by mass transport limitations; namely, the rapid consumption of electroactive species at the electrode/electrolyte interface outpaces their diffusion rate from the bulk solution. Furthermore, by applying the classical Randles-Sevcik equation to the experimental data, a high determination coefficient (R^2 = 0.9986) was achieved, confirming an excellent linear fit. Based on this linear regression, the diffusion coefficient of the electroactive species was calculated to be D = 1.26 x 10^{-7} cm^2/s, further substantiating the diffusion-limited kinetics of the synthesized thin-film electrodes during alkaline water electrolysis.

3.5 Calculation Electrochemical active surface area (ECSA)

The electrochemically active surface area (ECSA) was estimated based on the Cdl method. The following equations, (1) describe the mathematical approach utilized for the ECSA calculation.

$$ECSA = \frac{Cdl}{Cs} \qquad (1)$$

The double-layer capacitance (C_{dl}) was found to be 2.483 mF, which represents a significantly high value and underscores the exceptional electrocatalytic activity of the catalyst surface. The real surface area of the Ni-$W_{0.04}$ alloy synthesized on the Cu substrate was determined to be 62.08 cm^2. This value represents a significantly high ECSA, which subsequently allows for the calculation of the Roughness Factor (R_f)

$$\text{Roughness Factor} = \frac{\text{ECSA}}{\text{Ageo}} \qquad (2)$$

The roughness factor (R_f) was calculated to be 31.04, indicating that the ECSA is 18.92 times greater than the geometric surface area. This high R_f value confirms the significantly expanded active surface of the synthesized Ni-$W_{0.04}$ alloy.

Figure 10 shows the Gibbs free energy dependence for the hydrogen evolution reaction in the presence of Ni–W coatings. The energy landscape appears to consist of two stages: TS1 (the Volmer step) and TS2 (the Heyrovsky step). The first transition state (TS1) corresponds to water dissociation (Volmer step), while TS2, the second transition state, corresponds to hydrogen desorption (Heyrovsky step). As can be seen from the

figure, the Ni–$W_{0.01}$ sample, which showed a high Tafel slope value of 118 mV dec^{-1}, demonstrated lower activity in reducing the energy barrier compared to the other three samples.

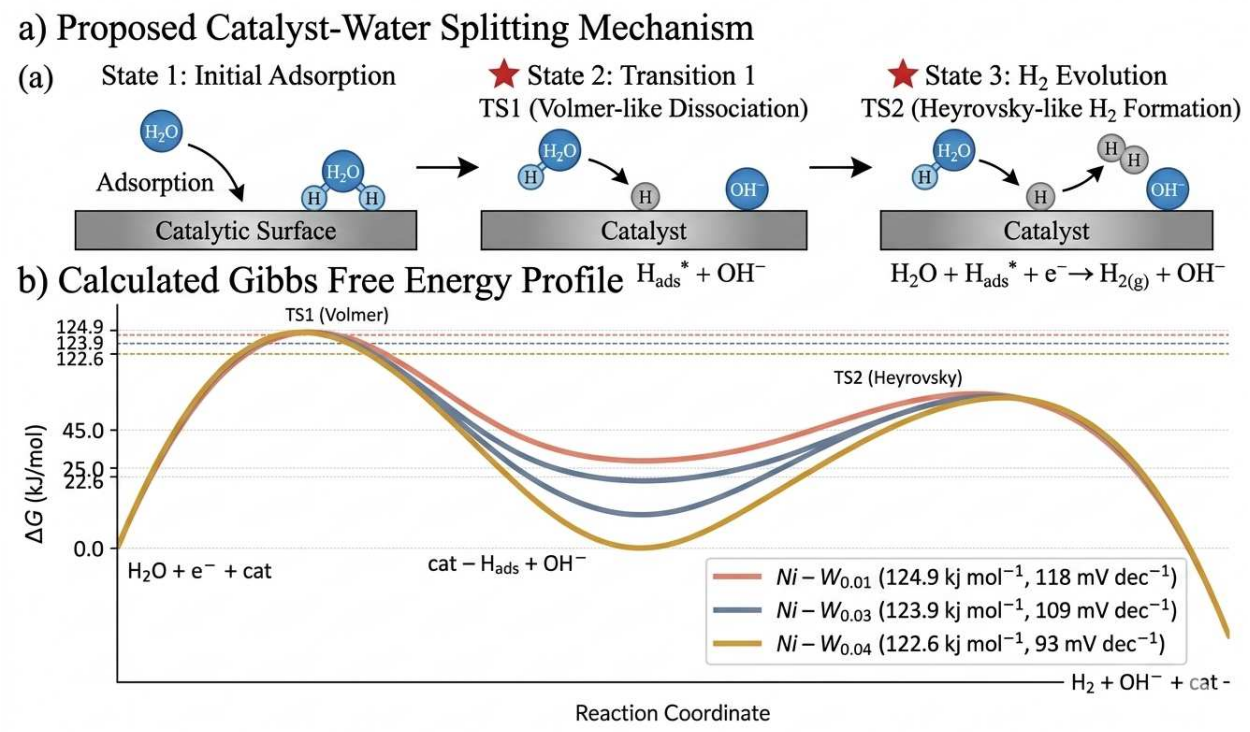


Fig.10 Schematic Gibbs free energy diagram for the hydrogen evolution reaction. Schematic representation of the Gibbs free energy profile for HER on Ni–W alloy electrodes with different Tafel slopes (118, 109 and 93 mV dec^{-1}), illustrating the relationship between energetics and catalytic activity.

The rate-determining step (RDS) is defined by the highest energy barrier (transition state) in each profile. The kinetic shift from the Volmer RDS (highest peak at TS1) to the Heyrovsky RDS (highest peak at TS2) for the optimal Ni–$W_{0.04}$ catalyst corresponds to the observed sharp decrease in the Tafel slope. Such a low Tafel slope value is associated with a large number of active sites and their high density in the Ni–$W_{0.04}$ sample compared to the other samples, making the Volmer step rate-limiting in this case. The energy profile clearly shows that water electrolysis on the Ni–$W_{0.04}$ electrode significantly lowers the activation energy of the hydrogen evolution reaction. It is also possible that the reduction in geometric surface area leads to an increase in the density of active sites per unit area, which also affects the electrocatalytic activity of the films.

This may explain the difference in Tafel slopes for two samples with identical composition but different geometric surface areas.

3.6 Electrochemical İmpendance Spectroscopy (EIS) Ni-W alloy coatings

Electrochemical Impedance Spectroscopy analysis (EIS) of Ni-W alloys and their corresponding equivalent circuit models in Figure 8

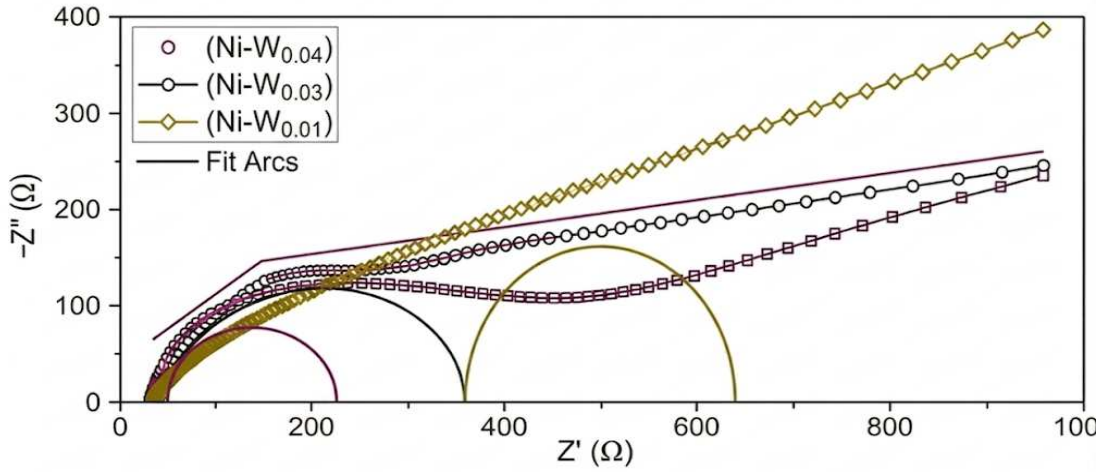


Fig. 11 Ni-W alloy coatings EIS analysis of Nyquist plots

Analysis of the presented Nyquist plots and their corresponding equivalent circuit models reveals a depressed semicircle in each spectrum, which is attributed to the Constant Phase Element (CPE). As a result of the electrochemical impedance spectroscopy (EIS) analysis, the CPE parameters for the Ni–$W_{0.04}$ catalyst were determined as Y_0 = 0.51 S s^n and n = 0.64. The significant deviation of the n parameter from the ideal capacitive behavior (n = 1) is attributed to the high surface roughness and heterogeneity of the coating. Consistent with the SEM analysis discussed above, an increase in the tungsten ion content leads to enhanced surface roughness, significantly affecting the roughness factor. Based on the EIS data, the Hydrogen Evolution Reaction (HER) proceeds most rapidly on the Ni–$W_{0.04}$ sample. The corresponding circuit model for this sample exhibits a single time constant, indicating a localized process occurring at the electrode-electrolyte interface. In contrast, the EIS analysis of the Ni–$W_{0.03}$ and Ni–$W_{0.04}$ alloys suggests the occurrence of multiple surface processes. For the Ni–W $_{0.03}$ sample, the transition to Warburg diffusion control over time reflects the increased complexity of the electrode

surface. Similarly, the Ni–$W_{0.04}$ alloy demonstrates two distinct surface processes, further highlighting the system's complexity. Finally, the Ni–$W_{0.01}$ sample shows that the process is diffusion-limited, exhibiting the lowest HER activity among the four samples.

3.7 Fourier-transform alternating current voltammetry (FTacV) analysis.

Recently, Fourier-transform alternating current voltammetry (FTacV) analysis has been widely used to investigate the kinetics of reactions with complex kinetic mechanisms, especially those involving water electrolysis, as it can provide extensive information about reaction kinetics [37,38]. Figure 9 shows the Fourier-transform alternating current voltammogram (FTacV) of the electrodeposited Ni–$W_{0.04}$ coating. Fig. 9. 1st and 2nd harmonic signals are given in the figure below.

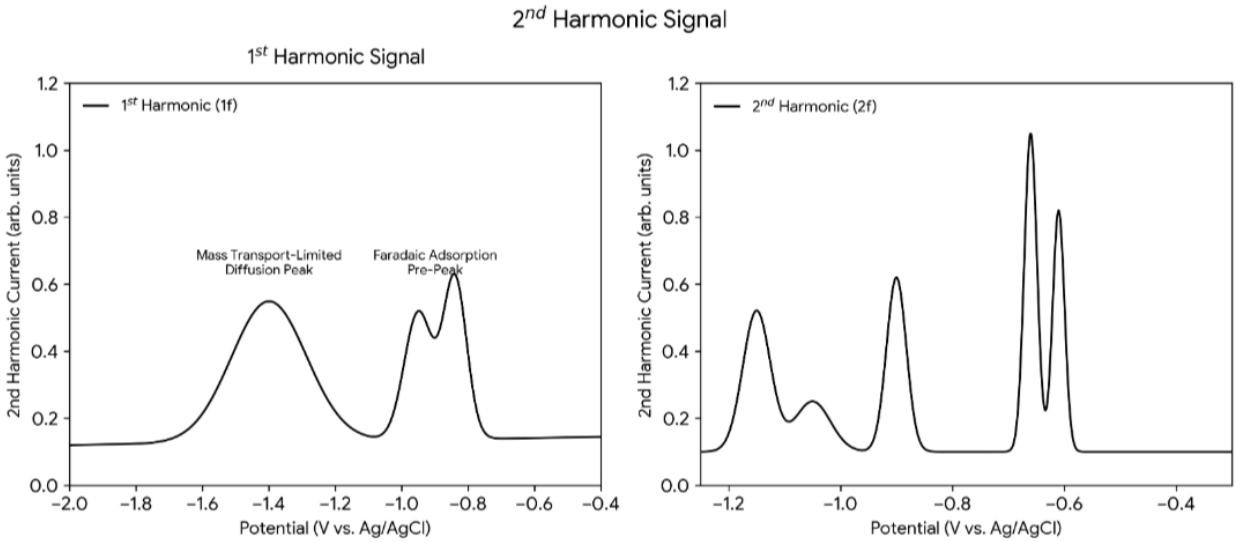


Fig.12.FTacV response of Ni–$W_{0.04}$ coating

The peaks in the figure correspond to hydrogen adsorption/desorption (H_{ads}) processes on different active sites. FTacV analysis performed at a frequency of 100 Hz and an amplitude of 10 mV shows that the Ni–$W_{0.04}$ electrocatalyst exhibits high activity in alkaline media. The second harmonic obtained from the FTacV analysis is also presented. The broad and widely separated peaks are associated with the amorphous nature of the sample. The asymmetric shape of the peaks indicates the irreversibility of the reaction, while their large number suggests that the reaction proceeds via multiple mechanisms [39]. The figure on the left displays the 1st harmonic signal, which represents a broader integrated form of the 2nd harmonics. The peaks between -0.8 V and -1.0 V indicate rapid kinetic processes, and as the potential shifts toward -1.4 V, mass transport processes become more dominant. The second graph presented on the right illustrates the second-harmonic analysis. The doublet peaks observed around -0.6 V and -0.65 V, which are relatively higher than the others, indicate the initial activation zone. These peaks

correspond to the initial hydrogen adsorption process. Meanwhile, the peak located around -0.9 V represents the Volmer step. Additionally, the peak at approximately -1.15 V signifies hydrogen desorption, whereas the peak at -1.2 V marks the onset of the diffusion-controlled stage.

3.8 The stability testing of Ni-W alloys samples and corrosion parameters.

Chronopotentiometry or chronoamperometry is a very important method for studying the long-term stability of electrocatalysts. Figure 10 shows the stability of the obtained alloys in 1 M KOH at a current density of 10 mA cm^{-2}. The prepared samples demonstrated stability for 24 hours, which can be considered a good result for laboratory testing.

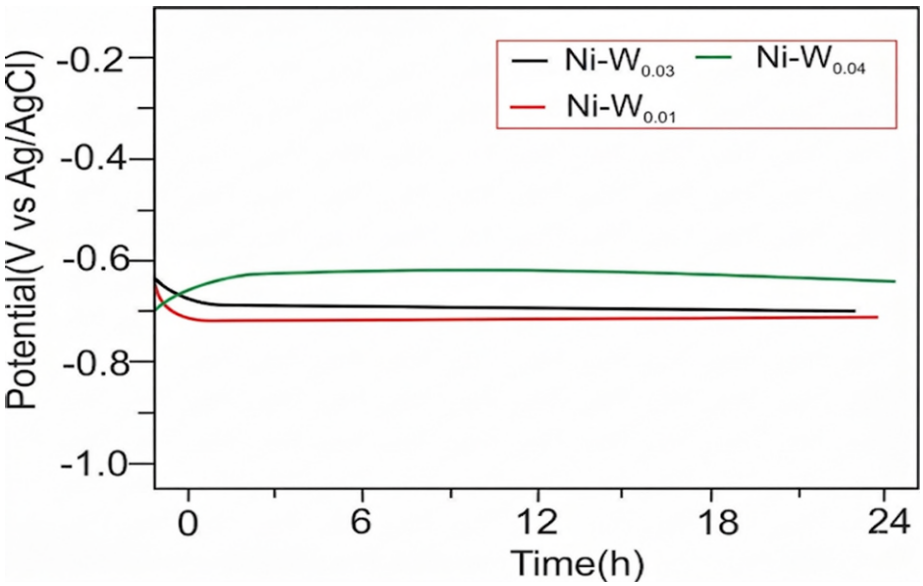


Fig.13. Stability test of Ni–W samples in 1 M KOH over 24 hours at 10 mA cm^{-2}.

Corrosion resistance and corrosion rate in the operating medium are important parameters for every electrocatalyst used in hydrogen evolution reactions. Since alkaline electrolytes are commonly used in industrial hydrogen production, the corrosion properties of the obtained films were investigated in an alkaline medium. Table 4 presents the corrosion parameters of the Ni–W alloys. As can be seen from the table, the Ni–$W_{0.04–0.5}$ alloy exhibits high corrosion resistance and a low corrosion rate in alkaline solution.The chronopotentiometric curves in Figure 9 for the four samples show that after stability testing in 1 M KOH for 10 hours, no degradation of the samples was observed, and the materials remained stable. Interestingly, although the optimized Ni–$W_{0.04}$ (blue curve) and Ni–$W_{0.04–0.5}$ (green curve) samples stabilized at a slightly more “noble” (positive) potential, this corresponds to the highest polarization resistance (1252.4 Ω·cm² and 1364 Ω·cm²)

and the lowest corrosion rate, as shown in Table 4 [40]. The values presented in Table 4 were calculated using the Stern-Geary equation.

$$Rp=\frac{B}{icor}$$

$$B=\frac{\beta a \beta c}{2.3(\beta a+\beta c)}$$

Table.4 Corrosion parameters of the Ni–W alloy coatings.

Alloys Ni-W test samples	E_{cor},obs(V)	J_{cor}(mA cm^{-2})	Area specific resistance A/Ohm cm^2	Corrosion rate, mm/Year
Ni-$W_{0.01}$	-0.243 V	6.666 x 10^{-5}	581.6	1.182
Ni-$W_{0.03}$	-0.420 V	5.662 x 10^{-5}	763.0	0.765
Ni-$W_{0.04}$	-0.636 V	4.523 x 10^{-5}	1252.4	0.528

This indicates a delicate balance in which high surface stability reduces excessive electrochemical overpotential, leading to the formation of a robust and durable catalyst surface that is ideally suited for continuous alkaline water electrolysis.

3.9 Comparison of the electrochemical performance of the developed electrocatalyst with previously reported literature

Table 5 presents a comparison of the Ni-$W_{0.04}$ alloy with other Ni-W-based samples. A comparison of the overpotential values at a current density of 100 mA cm^{-2}, alongside the Tafel slopes, reveals that the Ni-$W_{0.04}$ alloy exhibits superior catalytic activity for the HER compared to the other counter-samples. This confirms the reliability of the obtained results and demonstrates their comparability with previous literature. Furthermore, these findings validate that Ni-W alloys synthesized on copper foil can serve as highly efficient electrocatalysts for the HER.

Table.5 Comparison of electrocatalytic performance for Ni–W alloy coatings

Electrocatalyst	Media	Overpotential (η), (mV)	Tafel values mV dec^{-1}	References
PNiW5-6	1 M NaOH	$\eta_{100=331}$	111	43
Ni–23W	1 M KOH	$\eta_{100=556}$	-	41
Ni-$W_{0.04}$	1 M KOH	$\eta_{100=317}$	93	This work
Ni–32W	1 M KOH	$\eta_{100=534}$	-	41
Ni–6W	1 M KOH	$\eta_{50=668}$	168	42
CNiW10-1	1 M NaOH	$\eta_{50=341}$	92	43
Ni-W	1 M KOH	$\eta_{100=602}$	-	41

Conclusion

Ni–W alloy coatings were successfully fabricated via galvanostatic electrodeposition from a citrate electrolyte. The morphology, elemental composition, and electrochemical properties of the prepared alloys were systematically investigated using SEM, EDX, linear sweep voltammetry (LSV), and chronopotentiometric measurements. The as-deposited Ni–$W_{0.04}$ alloy coatings exhibited an amorphous structure; however, post-deposition annealing at 773 K for 1.5 hour induced phase transformation into a tetragonal Ni_4W intermetallic phase, as confirmed by XRD analysis. Long-term stability tests lasting 24 hours demonstrated that the alloys effectively maintained their initial structural integrity. Increasing the concentration of tungsten ions was found to exert a positive effect on the film thickness, electrocatalytic efficiency, and corrosion resistance of the alloys. Furthermore, EIS and FTacV analyses confirmed the superior performance of the Ni–$W_{0.04}$ alloy toward the hydrogen evolution reaction (HER). This outstanding electrocatalytic activity was further supported by the enhanced electrochemical active surface area (ECSA) and double-layer capacitance C_{dl} values. Notably, the elevation of these parameters led to a significant reduction in both the Tafel slope and the overpotentials at current densities of 10 and 100 mA cm^{-2}, thereby underscoring the exceptional overall efficiency of the developed electrocatalyst**.**

List of Abbreviations

SEM – Scanning Electron Microscopy

EDS – Energy Dispersive Spectroscopy

XRD – X-ray Diffraction

FTacV - Fourier-transform alternating current voltammetry

CPE - Constant Phase Element

EIS - Electrochemical İmpendance Spectroscopy

RDS - rate-determining step

Funding Statement

The authors received no financial support for this research.

Conflict of Interest

The authors declare that they have no conflict of interest.

Data Availability

The data supporting the findings of this study are available from the corresponding author upon reasonable request.

References

1.Roger, M. A. Shipman and M. D. Symes, Earth-abundant catalysts for electrochemical and photoelectrochemical water splitting, Nat. Rev. Chem., 2017, 1(1), 0003. . https://doi.org/10.1038/s41570-016-0003

2. C. Deviprasath, R. Rajendiran, O. L. Li and P. Kandasamy, Mn-Co bimetallic phosphate on electrodeposited PANI nanowires with composition modulated structural morphology for efficient electrocatalytic water splitting, Appl. Catal., B, 2021, 292, 120202. https://doi.org/10.1016/j.apcatb.2021.120202

3. L. Barreto, A. Makihira and K. Riahi, The hydrogen economy in the 21st century: A sustainable development scenario, Int. J. Hydrogen Energy, 2003, 28, 267–284. https://doi.org/10.1016/S0360-3199(02)00074-5

4. F. Mueller-Langer, E. Tzimas, K. Martin and S. Peteves, Techno-Economic Assessment of Hydrogen Production Processes for the Hydrogen Economy for the Short and Medium Term, Int. J. Hydrogen Energy, 2007, 32, 3797–3810. https://doi.org/10.1016/j.ijhydene.2007.05.027

5. K. Zeng and D. Zhang, Recent progress in alkaline water electrolysis for hydrogen production and applications, Prog. Energy Combust. Sci., 2010, 36(3), 307–326. https://doi.org/10.1016/j.pecs.2009.11.002

6. S. Paygozar, A. Sabour Rouh Aghdam, E. Hassanizadeh, R. Andaveh and G. Darband, Recent progress in non-noble metal-based electrocatalysts for urea-assisted electrochemical hydrogen production, Int. J. Hydrogen Energy, 2023, 48, 7219–7259. https://doi.org/10.1016/j.ijhydene.2022.10.203

7. Y. Li, R. Li, D. Wang, H. Xu, F. Meng, D. Dong, J. Jiang, J. Zhang, M. An and P. Yang, A review: Target-oriented transition metal phosphide design and synthesis for water splitting, Int. J. Hydrogen Energy, 2021, 46(7), 5131–5149. https://doi.org/10.1016/j.ijhydene.2020.11.022

8. C. Hu, L. Zhang and J. Gong, Recent progress made in the mechanism comprehension and design of electrocatalysts for alkaline water splitting, Energy Environ. Sci., 2019, 12(9), 2620–2645. https://doi.org/10.1039/C9EE01204H

9. H. Jiang, N. Cong, H. Jiang, M. Tian, Z. Xie, H. Fang, J. Han, Z. Ren and Y. Zhu, Dynamic hydrogen bubble template electrodeposition of Ru on amorphous Co support for electrochemical hydrogen evolution, Int. J. Hydrogen Energy, 2023, 48(57), 21599–21609. https://doi.org/10.1016/j.ijhydene.2023.02.197

10. A. O. Zeynalova, N. Sh. Soltanova, U. M. Gurbanova, R. G. Huseynova, A. Sh. Aliyev, D. B. Tagiyev, Electrodeposition of Ni-Co thin films from ammonia-chloride

electrolyte, Journal of Electrochemical Science and Engineering 15(3) 2025 2666. https://doi.org/10.5599/jese.2666

11. M. Khalid, B.S. De, S. Shahgaldi, Electrocatalytic lignin oxidation for hydrogen and fine chemical co-production using platinized nickel foam in a 3D printed reactor, DeCarbon 6 (2024) 100074. https://doi.org/10.1016/j.decarb.2024.100074

12. Y. Yao, J. Lyu, X. Li, C. Chen, F. Verpoort, J. Wang, Z. Pan, Z. Kou, A review of efficient electrocatalysts for the oxygen evolution reaction at large current density, DeCarbon 5 (2024) 100062. https://doi.org/10.1016/j.decarb.2024.100062

13. K. Zhang, R. Zou, Advanced transition metal-based OER electrocatalysts: current status, opportunities, and challenges, Small 17 (2021) 2100129. https://doi.org/10.1002/smll.202100129

14. L. Li, X. Cao, J. Huo, J. Qu, W. Chen, C. Liu, Y. Zhao, H. Liu, G. Wang, High valence metals engineering strategies of Fe/Co/Ni-based catalysts for boosted OER electrocatalysis, J. Energy Chem. 76 (2023) 195–213. https://doi.org/10.1016/j.jechem.2022.09.022

15. A. Brenner, Electrodeposition of Alloys: Principles and Practice, Elsevier, 2013. https://doi.org/10.1016/C2013-0-07073-5

16. Zhang X, Cui X, Sun Y, Qi K, Jin Z, Wei S, et al. Nanoporous sulfur-doped copper oxide (Cu_2OxS_1ex) for overall water splitting. ACS Appl Mater Interfaces 2018;10:745e52. https://doi.org/10.1021/acsami.7b14820

17. U. M. Gurbanova, D.M.Babanly, R. G. Huseynova, Aliyev, D. B. Tagiyev, Study of electrochemical deposition of Ni-Mo thin films from alkaline electrolytes, Journal of Electrochemical Science and Engineering 11(1) 2021 39 - 49. https://doi.org/10.5599/jese.912

18. Tian J, Liu Q, Cheng N, Asiri AM, Sun X. Self-supported Cu3P nanowire arrays as an integrated high-performance threedimensional cathode for generating hydrogen from water. Angew Chem 2014;126:9731e5. https://doi.org/10.1002/ange.201403123

19. C. Lupi, A. Dell'Era, M. Pasquali .Effectiveness of sodium citrate on electrodeposition process of Ni Co W alloys for hydrogen evolution reaction, International Journal of Hydrogen Energy, 2017, Pages 28766-28776. https://doi.org/10.1016/j.ijhydene.2017.09.139

20. Sriraman, K. R., Suryanarayana, C., & Froes, F. H. (2006). Structural features of electrodeposited nanocrystalline Ni–W alloys. Materials Science and Engineering A, 418, 303–311. https://doi.org/10.1016/j.msea.2005.11.032

21. Li, H., Wang, L., Zhang, Q., Surface Roughness and Electrochemical Performance Correlation in Nanostructured Catalysts, Nano Energy, 2017, 41, 390–398. https://doi.org/10.1016/j.nanoen.2017.09.042

22. Zhou, Y., Li, Y., Huang, Y., Effect of Electrode Surface Morphology on Electrocatalytic Activity for Water Splitting, Int. J. Hydrogen Energy, 2018, 43, 10504–10513. https://doi.org/10.1016/j.ijhydene.2018.03.011

23. N. Lot, G. Darband, Energy-Saving Electrochemical Hydrogen Production on Dynamic Hydrogen Bubble Template Electrodeposited Ni-Cu-Mn Nano-Micro Dendrite, J. Electrochem. Soc., 2022, 169, 096508. https://doi.org/10.1149/1945-7111/ac8c1d

24. S. L. Pasarakonda, S. Ponnada, M. S. Kiai, V. Duraisamy, H. Bindu G, A. Nowduri, S. M. S. Kumar and R. K. Sharma, Dual Metal Sites Coengineered Graphitic Carbon Nitride as Green Electrocatalyst for Highly Selective Overall Water Splitting—A Sustainable Approach, Energy Technol., 2025, 13(1), 2401577. https://doi.org/10.1002/ente.202401577

25. Zuraya Angeles-Olvera, D. Alfonso Crespo-Yapur , Oliver Rodríguez, Jorge L. Cholula-Díaz, Luz María Martínez and Marcelo Videa, Nickel-Based Electrocatalysts for Water Electrolysis, *Preprints* **2022.** https://doi.org/10.20944/preprints202201.0233.v2

26. Krischer, K.; Savinova, E.R., Fundamentals of Electrocatalysis. In Handbook of Heterogeneous Catalysis; Wiley-VCH Verlag GmbH & Co. KGaA, 2008; chapter 8, pp. 1873–1905. https://doi.org/10.1002/9783527610044.hetcat0082

27. Sarah M. Stratton, Shengjie Zhang, Matthew M. Montemore, Addressing complexity in catalyst design: From volcanos and scaling to more sophisticated design strategies, Surface Science Reports 78 (2023) 100597. https://doi.org/10.1016/j.surfrep.2023.100597

28.B. Xiong, W. Zhao, H. Tian, W. Huang, L. Chen and J. Shi, Nickel-Tungsten Nano-Alloying for High-Performance hydrogen Electro-Catalytic oxidation, Chem. Eng. J., 2022,432, 134189. https://doi.org/10.1016/j.cej.2021.134189

29. S. Ghobrial, D. Kirk and S. Thorpe, Nickel-Based Amorphous Alloys As Electrocatalyst Materials in Alkaline Water Electrolysis, ECS Meet. Abstr., 2017, MA2017-01, 1408.

30. M. Benaicha, M. Allam, A. Dakhouche and M. Hamla, Electrodeposition and Characterization of W-rich NiW Alloys from Citrate Electrolyte, Int. J. Electrochem. Sci., 2016, 11(9), 7605–7620.

31. Li, Y., Li, L., Li, W., Lu, L., Tian, L., Liu, Y., Su, C. & Tian, W., Preparation of Porous Ni–W Alloys Electrodeposited by Dynamic Hydrogen Bubble Template and Their

Alkaline HER Properties. Coatings, 14(8), 957 (2024). https://doi.org/10.3390/coatings14080957

32. Shen Y, Zhou YF, Wang D, Wu X, Li J, Xi JY. Nickel-copper alloy encapsulated in graphitic carbon shells as electrocatalysts for hydrogen evolution reaction. Adv Energy Mater. 2018;8(2): 1701759. https://doi.org/10.1002/aenm.201701759

33. Alsaiari, R. A., Abd-Ellah, A. A., Anwar, Z. M., Shata, S. S., Kamel, M. M. & Mostafa, N. Y., Electrodeposition and characterization of nanostructured composite Ni–W alloys for hydrogen evolution in basic media. RSC Advances, 15, 22322–22335 (2025). https://doi.org/10.1039/D5RA03136B

34.Xu, J., Li, Y., Wang, D., & Chen, Z. (2019). Ni–W alloy as efficient electrocatalyst for hydrogen evolution reaction in alkaline media. Electrochimica Acta, 297, 1–10. https://doi.org/10.1016/j.electacta.2018.12.045

35. Zhang, T., Li, H., Chen, Y., & Wang, X. (2020). Enhanced electrocatalytic hydrogen evolution on nanostructured Ni–W alloy. ACS Catalysis, 10(12), 6734–6742. https://doi.org/10.1021/acscatal.0c01657

36.Kibsgaard, J., & Jaramillo, T. F. (2014). Molybdenum phosphosulfide: An active, acid-stable, earth-abundant catalyst for the hydrogen evolution reaction. Angewandte Chemie International Edition, 53(52), 14433–14437. https://doi.org/10.1002/anie.201408690

37. Snitkoff-Sol, R. Z.; Bond, A. M.; Elbaz, L. Fourier-Transformed Alternating Current Voltammetry (FTacV) for Analysis of Electrocatalysts. ACS Catalysis 2024, 14 (10), 7576–7588. https://doi.org/10.1021/acscatal.4c01526

38. Natalia G. Baranska, Bryn Jones, Mark R. Dowsett, Chris Rhodes, Darrell M. Elton, Jie Zhang,Alan M. Bond, David Gavaghan, Henry O. Lloyd-Laney, and Alison Parkin, Practical Guide to Large Amplitude Fourier-Transformed Alternating Current Voltammetry_What, How, and Why, ACS Meas. Sci. Au 2024, 4, 418−431. https://doi.org/10.1021/acsmeasuresciau.4c00008

39. Teng Zhang, Yi-Hong Yu, Chuang-Wei Liu, Gao-Wu Qin, Song Li, Constructing Ni_4W/WO_3/NF with strongly coupled interface for hydrogen evolution in alkaline media, Rare Met. (2023) 42(12):3945–3951. https://doi.org/10.1007/s12598-023-02362-5

40. Mohamed Benaicha, Mahdi Allam , Achour Dakhouche, Meriem Hamla, Electrodeposition and Characterization of W-rich NiW Alloys from Citrate Electrolyte, Int. J. Electrochem. Sci., 11(2016) 7605 – 7620, doi: 10.20964/2016.09.17

41. M. Abel, J. Z´´achensk´a, E. Dobrocka and M. Zemanov´a, Electrocatalytic properties of pulse plated Ni-W alloy coatings in alkaline electrolytes, Trans. IMF, 2021, 99, 23–28.

42.Alsaiari, R. A., Abd-Ellah, A. A., Anwar, Z. M., Shata, S. S., Kamel, M. M., & Mostafa, N. Y. (2025). Electrodeposition and characterization of nanostructured composite Ni–W alloys for hydrogen evolution in basic media. *RSC Advances*, *15*(28), 22322–22335. https://doi.org/10.1039/D5RA03136B

43. Y. Li, L. Li, W. Li, L. Lu, L. Tian, Y. Liu, C. Su and W. Tian, Preparation of Porous Ni-W Alloys Electrodeposited by Dynamic Hydrogen Bubble Template and Their Alkaline HER Properties, Coatings, 2024, 14(8), 957